

Symmetry-Broken Perturbation Theory to Large Orders in Antiferromagnetic Phases

Renaud Garioud,^{1,2,*} Fedor Šimkovic IV,^{1,2} Riccardo Rossi^{3,4}, Gabriele Spada^{5,6}Thomas Schäfer⁷, Félix Werner⁵, and Michel Ferrero^{1,2}¹*CPHT, CNRS, École Polytechnique, Institut Polytechnique de Paris, 91128 Palaiseau, France*²*Collège de France, 11 place Marcelin Berthelot, 75005 Paris, France*³*Institute of Physics, École Polytechnique Fédérale de Lausanne (EPFL), CH-1015 Lausanne, Switzerland*⁴*Sorbonne Université, CNRS, Laboratoire de Physique Théorique de la Matière Condensée, LPTMC, F-75005 Paris, France*⁵*Laboratoire Kastler Brossel, École Normale Supérieure - Université PSL, CNRS, Sorbonne Université, Collège de France, 75005 Paris, France*⁶*Pitaevskii BEC Center, CNR-INO and Dipartimento di Fisica, Università di Trento, I-38123, Trento, Italy*⁷*Max-Planck-Institut für Festkörperforschung, Heisenbergstraße 1, 70569 Stuttgart, Germany* (Received 23 June 2023; revised 12 March 2024; accepted 7 May 2024; published 14 June 2024)

We introduce a spin-symmetry-broken extension of the connected determinant algorithm [Riccardo Rossi, Determinant diagrammatic Monte Carlo algorithm in the thermodynamic limit, *Phys. Rev. Lett.* **119**, 045701 (2017)]. The resulting systematic perturbative expansions around an antiferromagnetic state allow for numerically exact calculations directly inside a magnetically ordered phase. We show new precise results for the magnetic phase diagram and thermodynamics of the three-dimensional cubic Hubbard model at half-filling. With detailed computations of the order parameter in the low to intermediate-coupling regime, we establish the Néel phase boundary. The critical behavior in its vicinity is shown to be compatible with the O(3) Heisenberg universality class. By determining the evolution of the entropy with decreasing temperature through the phase transition we identify the different physical regimes at $U/t = 4$. We provide quantitative results for several thermodynamic quantities deep inside the antiferromagnetic dome up to large interaction strengths and investigate the crossover between the Slater and Heisenberg regimes.

DOI: 10.1103/PhysRevLett.132.246505

In strongly correlated materials, such as high temperature superconducting copper oxides or iron-based pnictides, the interactions between electrons yield intricate phase diagrams, exhibiting, e.g., magnetically or charge-ordered phases, superconductivity, or Mott insulating behaviors. Understanding the properties of these different phases, their interplay and driving mechanisms is one of the outstanding challenges of modern condensed matter theory.

From the theoretical point of view, one of the simplest models to investigate phase transitions is the three-dimensional cubic Hubbard model [1–6] given by the Hamiltonian

$$\hat{\mathcal{H}} = -t \sum_{\langle i,j \rangle} \sum_{\sigma} \hat{c}_{i\sigma}^{\dagger} \hat{c}_{j\sigma} + U \sum_i \hat{n}_{i\uparrow} \hat{n}_{i\downarrow} - \mu \sum_{i\sigma} \hat{n}_{i\sigma}, \quad (1)$$

where t is the hopping amplitude between nearest-neighbor sites $\langle i, j \rangle$ on a cubic lattice, $U \geq 0$ the on-site Coulomb interaction, μ the chemical potential, $\hat{n}_{i\sigma} = \hat{c}_{i\sigma}^{\dagger} \hat{c}_{i\sigma}$ and $\hat{c}_{i\sigma}^{\dagger}$ creates an electron on site i with spin σ . At half-filling ($\mu = U/2$), the ground state has antiferromagnetic long-range spin order. In three dimensions this SU(2) symmetry-broken phase survives up to the Néel temperature $T_N(U)$ above which the system becomes paramagnetic. While there is qualitative understanding of the mechanisms that

produce the antiferromagnetic order both at weak and strong coupling, obtaining unbiased quantitative results, especially close to the phase transition and inside the ordered phase, is still very challenging [7–19]. Therefore, despite its apparent simplicity, the Hubbard model on the cubic lattice is an ideal platform to explore the potential of new algorithms before engaging in the study of more realistic systems. The model was realized in cold-atomic experiments on optical lattices where antiferromagnetism is under active investigation [20–28].

The main challenge for theoretical approaches based on finite size lattices is to properly account for the increasing correlation length in the vicinity of a second order phase transition, and, as such, to extrapolate to the thermodynamic limit. In that respect, the diagrammatic Monte Carlo approach [29–31] is very promising as it offers the possibility to investigate a system directly in the thermodynamic limit. The method stochastically computes the coefficients a_k appearing in the perturbative expansion in U of a physical observable, $\mathcal{A}(U) = \sum_k a_k U^k$ in the simplest formulation. The computational cost rapidly increases with increasing perturbation orders and only so many coefficients can be computed before the statistical variance becomes overwhelming. Nevertheless, important improvements [32,33] make it now possible to reach perturbation

orders as large as 10–12. In the context of the repulsive Hubbard model, the diagrammatic Monte Carlo method has already been successfully applied to nonperturbative regimes in the two-dimensional square lattice [31,34–43].

In the usual formulation, the perturbation series is constructed starting from the noninteracting ($U = 0$) SU(2)-symmetric solution of Eq. (1). This allows to obtain results for the interacting system in its paramagnetic regime. As the phase transition to the antiferromagnetic state is approached, however, the resummation of the series becomes increasingly difficult. The reason is that a second-order phase transition happening at $U = U_c$ is accompanied by a singularity in the complex- U plane for observables $\mathcal{A}(U)$ that show a non-analyticity at U_c . Consequently, investigating the antiferromagnetic transition in the cubic Hubbard model can only be done from temperatures above and not too close to the Néel temperature T_N . Very recently, the spin structure factor perturbation series has been computed this way in the paramagnetic phase of the cubic Hubbard model [42]. Assuming the critical behavior in the vicinity of the phase transition, the authors were able to accurately compute T_N in the weak-to-intermediate coupling regime both at half-filling and at finite doping. This approach is, however, not able to address the properties of the model inside the ordered phase.

In this Letter, we take a complementary approach and compute the perturbation series for physical observables within the antiferromagnetic phase of the cubic half-filled Hubbard model. We show that our broken-symmetry approach to perturbative expansions is a powerful tool for studying magnetically ordered phases and phase transitions. Our results are obtained directly in the thermodynamic limit and, thus, do not involve any finite size scaling. We document the vanishing of the magnetic order parameter at T_N and the corresponding critical exponent β and report and discuss the behavior of the double occupancy, grand potential, and entropy across the phase transition and inside the ordered phase.

Method.—The possibility to construct symmetry-broken perturbation series comes from a flexibility in the choice of the starting point around which the perturbation is expanded. This freedom has been extensively applied to diagrammatic Monte Carlo computations in the nonmagnetic phase to improve the convergence properties of the series [39–41,44–52]. Very recently, it has been used to construct a perturbation theory around a BCS state and inside the superconducting phase of the attractive Hubbard model [53]. Here, we follow similar steps and introduce the modified Hamiltonian

$$\hat{\mathcal{H}}_\xi = -t \sum_{\langle i,j \rangle} \sum_{\sigma} \hat{c}_{i\sigma}^\dagger \hat{c}_{j\sigma} - \xi \frac{U}{2} \sum_{i\sigma} \hat{n}_{i\sigma} + (1 - \xi)h \sum_i p_i \hat{S}_i^z + \xi U \sum_i \hat{n}_{i\uparrow} \hat{n}_{i\downarrow}, \quad (2)$$

where $\hat{S}_i^z = (\hat{n}_{i\uparrow} - \hat{n}_{i\downarrow})/2$ and $p_i = \pm 1$ depending on whether i belongs to one or the other sublattice of the

bipartite cubic lattice. Observables are expressed as perturbation series in ξ and physical results are recovered for $\xi = 1$, where both Hamiltonians become equivalent, $\hat{\mathcal{H}}_{\xi=1} = \hat{\mathcal{H}}$. The perturbation series in ξ is built around a state that breaks the SU(2) spin rotation symmetry of the original Hamiltonian. Indeed, $\hat{\mathcal{H}}_{\xi=0}$ describes free electrons in a staggered external magnetic field h . Because this state breaks the symmetry from the start, the perturbation series can describe a magnetically ordered phase without the need of undergoing a phase transition. Accordingly, singularities in the complex- ξ plane associated with the phase transition are avoided.

We compute the coefficients of the perturbation series with the CDet [32] algorithm using a rejection-free many-configuration Monte Carlo [54] as well as a fast principal minor algorithm [55,56] to improve the speed of the determinant calculations. The series are evaluated with different resummation techniques [57,58] that serve as a basis to determine the error bars of our results, see Supplemental Material [59]. While the diagrammatic expansion can be formulated directly in the thermodynamic limit, in practice, we use a system with $L^3 = 20^3$ sites for our computations. We have carefully checked that this is large enough to avoid finite-size effects, even in the vicinity of the phase transition, as discussed in the Supplemental Material [59]. In the following, we will denote this spin symmetry-broken algorithm by CDet(AFM).

In the Hamiltonian of Eq. (2), the field h can be chosen arbitrarily and different choices for h define different series. In order to obtain the best convergence and to cross-check different results, we have systematically computed several values in the range $0 \leq h \leq h_{\text{MF}}$, where h_{MF} is the effective field found in the mean-field solution of Eq. (1). In the following, we will parametrize $h = \alpha h_{\text{MF}}$ with $0 \leq \alpha \leq 1$. Note that when $\alpha = 0$, the perturbation series is the usual expansion limited to the paramagnetic regime. Details about the important role of α on the convergence speed of the series can be found in the Supplemental Material [59]. We also include tables with the actual values of α that were used in our calculations.

For our analysis we compute the double occupancy $D = \langle \hat{n}_{i\uparrow} \hat{n}_{i\downarrow} \rangle = E_{\text{pot}}/U$, the staggered magnetization $m = \langle \hat{n}_{i\uparrow} - \hat{n}_{i\downarrow} \rangle$ (which is the order parameter for the Néel phase transition) and the grand potential per lattice site $-\Omega/L^3 = P$, where L is the linear system size of the cubic lattice, and P the thermodynamic pressure. The grand potential computations enable us to determine the entropy density and magnetization through

$$s = -\frac{\partial \Omega}{L^3 \partial T} \quad m = -\frac{\partial \Omega}{L^3 \partial H_{\text{ext}}} \Big|_{H_{\text{ext}}=0}, \quad (3)$$

where H_{ext} is an external Zeeman staggered field whose sign alternates on neighboring sites in the form of an

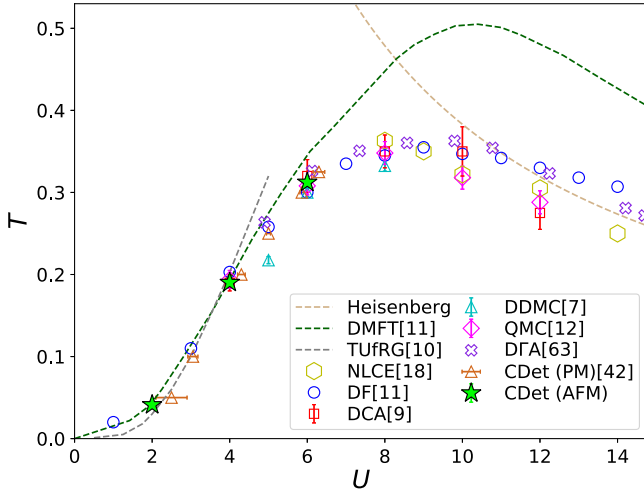


FIG. 1. Comparison of the Néel temperature $T_N(U)$ (lime green stars), obtained with the symmetry broken CDet(AFM), with other numerical methods. References for the numerical methods data are indicated in the legend.

additional term to the Hubbard Hamiltonian Eq. (1): $H_{\text{ext}} \sum_i p_i \hat{S}_i^z$. All energies are expressed in units of the hopping amplitude $t = 1$.

Phase diagram and universality class.—We start our study by determining the Néel temperature for different values of the interaction in order to establish the magnetic phase diagram of the system.

In Fig. 1 we compare our values for the critical temperature $T_N(U)$ from CDet(AFM) against numerous other numerical methods [7,9–12,18,42,63]. The Néel temperature is expected to increase with increasing interaction at small U since the transition is driven by the Slater mechanism [64] and reaches a maximum in the intermediate coupling around $U \simeq 6$ –10, before decreasing like $T_N \simeq 0.946J$ [65] in the high- U Heisenberg limit, where $J = 4t^2/U$ is the superexchange coupling. We have been able to determine the critical temperature up to an intermediate coupling strength of $U = 6$. For $U > 6$, regarding the magnetization, we experience increased difficulty in resumming our perturbation series and loss of Monte Carlo accuracy in the critical region close to the phase transition.

The values of the Néel temperature displayed in Fig. 1 are obtained from the computation of the magnetization as a function of temperature $m(T)$, which we show in Fig. 2. The order parameter m indicates the phase transition by assuming a nonzero value when decreasing the temperature: $T_N(U = 2) = 0.0425(25)$, $T_N(U = 4) = 0.1925(25)$, and $T_N(U = 6) = 0.32(1)$. Thanks to our high precision data, we manage to compute directly the β critical exponent from the critical behavior $m(T) \simeq a(T_N - T)^\beta$. The obtained values for the critical exponent Fig. 2 (top right) compare remarkably well to the literature values for the O(3) Heisenberg universality class [8,11,66,67]. They establish the first direct computations of the β critical exponent on a

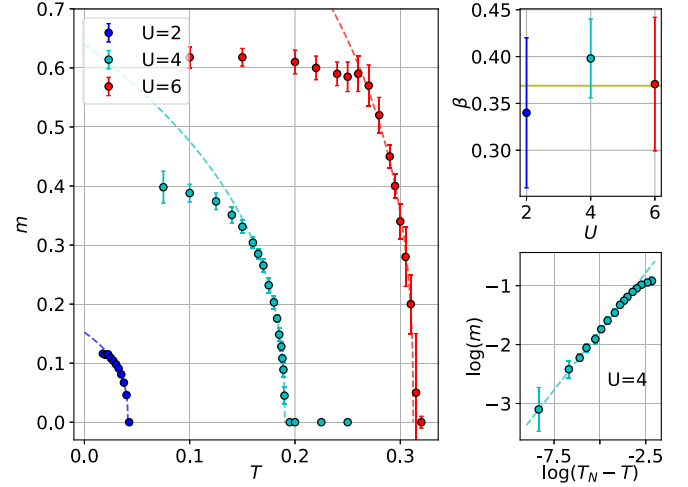


FIG. 2. Magnetization and critical behavior. Left panel: Magnetization m as a function of temperature T for three different values of the interaction U . The dashed curves represent the critical behavior as determined from our data close to the critical temperature fitted with the formula: $m(T) \simeq a(T_N - T)^\beta$. Top right panel: Critical exponent obtained from the three magnetization curves. The gold horizontal band corresponds to the theoretically predicted value of β for the O(3) Heisenberg universality class in [66]. Lower right panel: magnetization as a function of $T_N - T$ at $U = 4$ on a log-log scale. T_N is determined with the critical behavior fit from the left panel. The dashed line corresponds to the fitting curve on the left panel.

fermionic lattice and in the thermodynamic limit. As shown in Fig. 1, the values that we obtain for the Néel temperature compare well with paramagnetic DiagMC [42] and DCA extrapolated to infinite cluster size [9], as well as to the recently improved dynamical vertex approximation DGA [63], but are out of the error bounds obtained by finite-size scaling of $L \leq 10$ DDMC data [7]. The critical region, defined as the temperature range $T \in [T_N - \delta T, T_N]$, where $m(T) = a(T_N - T)^\beta$ is a good fit to our data, is of the order of $\delta T \simeq 0.025$ for $U \geq 4$. At such values of the interaction, the magnetization and the other thermodynamic quantities (see Figs. 3 and 4) only have a variation in a temperature interval $\delta T \simeq 0.1$ below T_N before they essentially saturate to their low temperature value.

Double occupancy.—The signatures of the phase transition can also be read from the double occupancy, shown in Fig. 3. At $U = 4$, we observe a sharp change of behavior of the double occupancy at a temperature in good agreement with the value of the Néel temperature determined in Fig. 2. Given the critical exponent $\alpha = -0.1336(15)$ for the O(3) Heisenberg universality class [66], we only expect a divergence in the second derivative of the double occupancy with respect to the temperature. At this value of the interaction, the double occupancy increases with decreasing temperature in the paramagnetic phase because of the Pomeranchuk effect [68–72]. It decreases in the antiferromagnetic phase which is consistent with the Slater

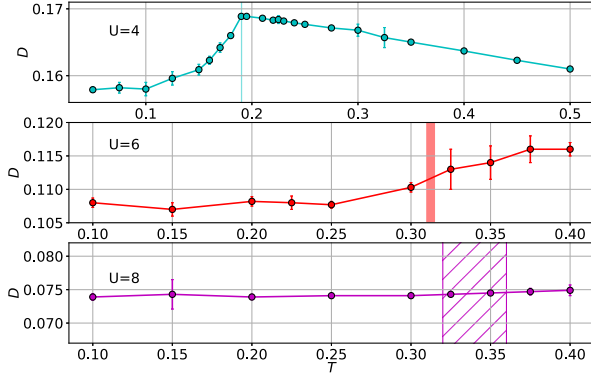


FIG. 3. Double occupancy D as a function of temperature for three different values of the interaction U . The vertical bands at $U = 4$ and $U = 6$ correspond to the estimate of the Néel temperature from our study, while the hashed area at $U = 8$ is an estimate of the Néel transition from other numerical methods displayed in Fig. 1.

mechanism expected at small interaction: The ordered phase is stabilized because of a gain in potential energy $E_{\text{pot}} = UD$ and, hence, a lowering of double occupancy at fixed interaction, as also observed, e.g., in DCA calculations [73]. At higher values of U the double occupancy curve flattens, and within our accuracy, we are not able to document the nonanalyticity of the double occupancy at the Néel temperature. We do not observe significant changes of the double occupancy around the Néel temperature at $U = 8$ within the 10^{-2} relative accuracy of our computation. Further work with better sensitivity or studying the kinetic energy would be needed to clearly document the change from a Slater to a Heisenberg regime with a kinetic-energy driven phase transition, as was done in DMFT and extensions thereof in [74–76].

Grand potential.—The grand potential at $U = 4$ is displayed in Fig. 4. In order to evaluate the entropy density from Eq. (3) we suppose a polynomial behavior of the grand potential with temperature. Since $\Omega(T) - \Omega(T = 0) \propto T^4$ for $T \rightarrow 0$, we fit the $T < T_N$ data with the expression $-\Omega(T) = -\Omega(T = 0) + aT^4 + bT^5 + cT^6$ (cyan curve). At $T > T_N$ we expect a quadratic behavior in the degenerate Fermi liquid regime. The data are well fitted by the expression $-\Omega/L^3(T) = d + eT^2$ (yellow curve). We impose continuity up to first order derivative at $T = T_N$. At higher temperatures $T \geq 0.4$ the grand potential becomes almost linear in temperature $-\Omega(T) \simeq \log(4)T$. The entropy density is then extracted with a finite difference scheme. These different behaviors of the grand potential lead to different physical regimes for the evolution of the entropy density with temperature. In the AFM phase the entropy density varies as $s \propto T^3$ at small temperatures. For temperatures just above the transition $T \in [T_N, 0.35]$ the entropy density increases linearly with the temperature which is a signature of a metallic behavior of the system in

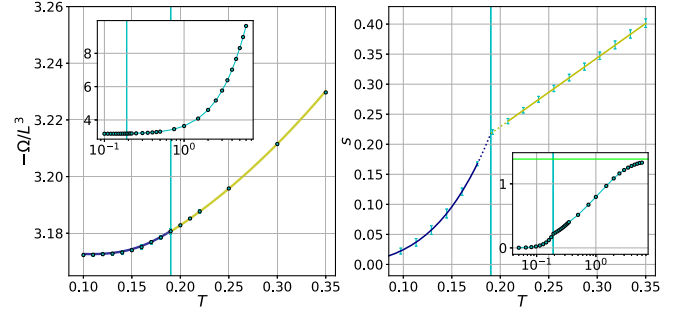


FIG. 4. Left panel: Grand potential density $-\Omega/L^3$ as a function of temperature T at interaction $U = 4$. When not visible the error bar is smaller than the markers. Right panel: Entropy density s as a function of temperature T obtained as derivative of the grand potential fitting curves (see text). The cyan error bars give the error on the entropy curve. We do not have enough data close to the Néel temperature to resolve the critical behavior of the entropy, and the entropy curve is dashed in this region. The insets are the same plots on a log scale for the x axis, and on a larger temperature range. The lime green horizontal line indicates the high temperature limit $s = \log(4)$. On both panels the vertical lines correspond to the value of the Néel temperature obtained in Fig. 2.

this part of the phase diagram. At higher temperatures of the order of the interaction $T \sim U = 4$ the entropy density saturates to $s(T \rightarrow +\infty) = \log(4)$.

Magnetically saturated regime at low T .—We are now interested in the low temperature properties of the system where the magnetization has reached saturation. We have observed earlier that the magnetization only changes significantly in a shell of size $\delta T \sim 0.1$ below the Néel temperature, so that the region with saturated magnetization represents an important part of the antiferromagnetic dome.

Direct computations of the magnetization become problematic for $U > 6$ because the associated series are difficult to resum. At strong interaction and low temperatures the expansion series for the grand potential turn out to be easier to resum towards a controlled accurate numerical result. Hence in this temperature regime it is more practical to compute the grand potential density and extract the magnetization as its variation with the external field as stated in Eq. (3). More details, and the associated computations are shown in the Supplemental Material [59].

The directly computed magnetization compares well with differentiating the grand potential as shown in Fig. 5. For $U \geq 6$ we observe no difference between the $T = 0.1$ and $T = 0.2$ curves which shows that the magnetization is already saturated at its zero temperature value. The magnetization will eventually have a maximum with respect to U , and our results show that it is situated at larger values of the interaction for $U > 18$.

The variations of the double occupancy with the interaction at low temperatures are shown in Fig. 5. In the paramagnetic phase the double occupancy is decreasing

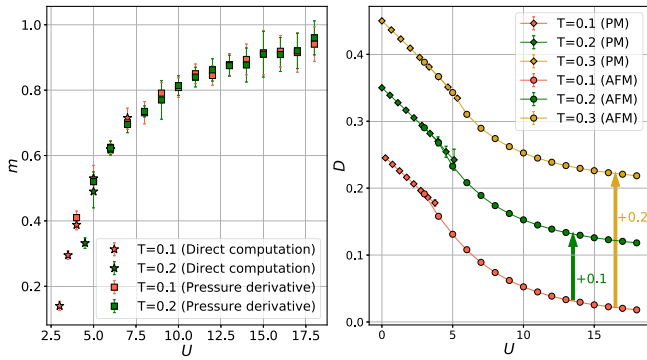


FIG. 5. Left panel: Magnetization as a function of the interaction U for two different values of the temperature. The square markers are obtained through direct computation of the order parameter as in Fig. 2. The round markers are obtained by numerically differentiating the grand potential density at an external field $H_{\text{ext}} \rightarrow 0$, see Eq. (3). Right panel: Double occupancy D as a function of the interaction U for three different values of the temperature. For better visibility the data at $T = 0.2$ ($T = 0.3$) is shifted by $+0.1$ ($+0.2$). The square markers are in the paramagnetic phase and are obtained with the paramagnetic (PM) CDet algorithm (no symmetry-breaking at $\alpha = 0$). The round markers are obtained with the antiferromagnetic symmetry-broken CDet with $\alpha \neq 0$ (AFM).

quasi-linearly with the interaction. In the vicinity of the phase transition we observe good agreement between results for the paramagnetic and symmetry-broken computations. As expected, at the transition U_c we observe a sharp change of behaviour of the double occupancy, and these results can be used to estimate the value of the critical interaction at fixed temperature. The double occupancy decreases faster with increasing interaction when entering the AFM phase which is consistent with the Slater mechanism at the transition for values of the critical interaction $U_c < 6$. In the antiferromagnetic phase the double occupancy is a convex function of the interaction which decays slowly to zero at infinite interaction. At $U > 7$ we cannot distinguish between the different temperatures within our accuracy as expected from Fig. 3. This is consistent with the fact that we do not observe clear signatures of the phase transition towards the paramagnetic phase in the double occupancy at large interactions.

Conclusions.—To conclude, we have applied the new algorithmic developments of the symmetry-broken CDet approach to produce the first high order diagrammatic computations inside an antiferromagnetic phase and directly in the thermodynamic limit. We have provided a quantitative description of the antiferromagnetic phase of the cubic half-filled Hubbard model. After determining the critical behavior of the system and its phase diagram we have reported resummed results at small temperatures deep inside the antiferromagnetic dome up to high interactions $U = 18$. We have shown that the diagrammatic Monte Carlo approach is a powerful tool to study the

physics of ordered systems with no need for an embedding scheme or system size extrapolation. A more advanced, nonlinear chemical-potential shift combined with other CDet extensions [41] may lead to further improvements for describing the critical behavior in the strong-coupling Heisenberg part of the antiferromagnetic dome. This symmetry-broken expansion could be applied to incommensurate orders in the doped regime, similarly to what was done in the paramagnetic phase [42] or with embedding methods [67]. Another interesting possibility would be to extend our study by including an anisotropic hopping term $t_{\text{perp}} < t$ in the z direction (similarly to what was done in [77]) in order to investigate how the magnetic properties are modified as the two-dimensional limit is approached. This application would be especially relevant for the physics of cuprate superconductors.

The authors are grateful to A. Georges, A. J. Kim, E. Kozik, C. Lenihan, G. Rohringer, and J. Stobbe for valuable discussions. This work was granted access to the HPC resources of TGCC and IDRIS under the allocations A0150510609 attributed by GENCI (Grand Equipement National de Calcul Intensif). It has also used high performance computing resources of IDCS (Infrastructure, Données, Calcul Scientifique) under the allocation CPHT (Centre de Physique Théorique) 2023. This work has been supported by the Simons Foundation within the Many Electron Collaboration framework. G. S. acknowledges support from Provincia Autonoma di Trento.

*garioudrenaud@gmail.com

- [1] J. Hubbard and Brian Hilton Flowers, Electron correlations in narrow energy bands, *Proc. R. Soc. A* **276**, 238 (1963).
- [2] J. Hubbard and Brian Hilton Flowers, Electron correlations in narrow energy bands III. An improved solution, *Proc. R. Soc. A* **281**, 401 (1964).
- [3] Junjiro Kanamori, Electron correlation and ferromagnetism of transition metals, *Prog. Theor. Phys.* **30**, 275 (1963).
- [4] Martin C. Gutzwiller, Effect of correlation on the ferromagnetism of transition metals, *Phys. Rev. Lett.* **10**, 159 (1963).
- [5] Daniel P. Arovas, Erez Berg, Steven A. Kivelson, and Srinivas Raghu, The Hubbard model, *Annu. Rev. Condens. Matter Phys.* **13**, 239 (2022).
- [6] Mingpu Qin, Thomas Schäfer, Sabine Andergassen, Philippe Corboz, and Emanuel Gull, The Hubbard model: A computational perspective, *Annu. Rev. Condens. Matter Phys.* **13**, 275 (2022).
- [7] E. Kozik, E. Burovski, V. W. Scarola, and M. Troyer, Néel temperature and thermodynamics of the half-filled three-dimensional Hubbard model by diagrammatic determinant Monte Carlo, *Phys. Rev. B* **87**, 205102 (2013).
- [8] G. Rohringer, A. Toschi, A. Katanin, and K. Held, Critical properties of the half-filled Hubbard model in three dimensions, *Phys. Rev. Lett.* **107**, 256402 (2011).

- [9] P. R. C. Kent, M. Jarrell, T. A. Maier, and Th. Pruschke, Efficient calculation of the antiferromagnetic phase diagram of the three-dimensional Hubbard model, *Phys. Rev. B* **72**, 060411(R) (2005).
- [10] J. Ehrlich and C. Honerkamp, Functional renormalization group for fermion lattice models in three dimensions: Application to the Hubbard model on the cubic lattice, *Phys. Rev. B* **102**, 195108 (2020).
- [11] Daniel Hirschmeier, Hartmut Hafermann, Emanuel Gull, Alexander I. Lichtenstein, and Andrey E. Antipov, Mechanisms of finite-temperature magnetism in the three-dimensional Hubbard model, *Phys. Rev. B* **92**, 144409 (2015).
- [12] R. Staudt, M. Dzierzawa, and A. Muramatsu, Phase diagram of the three-dimensional Hubbard model at half filling, *Eur. Phys. J. B* **17**, 411 (2000), .
- [13] A. N. Tahvildar-Zadeh, J. K. Freericks, and M. Jarrell, Magnetic phase diagram of the Hubbard model in three dimensions: The second-order local approximation, *Phys. Rev. B* **55**, 942 (1997).
- [14] G. Rohringer and A. Toschi, Impact of nonlocal correlations over different energy scales: A dynamical vertex approximation study, *Phys. Rev. B* **94**, 125144 (2016).
- [15] Sergei Isakov and Emanuel Gull, Phase transitions in partial summation methods: Results from the three-dimensional Hubbard model, *Phys. Rev. B* **105**, 045109 (2022).
- [16] G. Rohringer, H. Hafermann, A. Toschi, A. A. Katanin, A. E. Antipov, M. I. Katsnelson, A. I. Lichtenstein, A. N. Rubtsov, and K. Held, Diagrammatic routes to nonlocal correlations beyond dynamical mean field theory, *Rev. Mod. Phys.* **90**, 025003 (2018).
- [17] Lorenzo Del Re and Alessandro Toschi, Dynamical vertex approximation for many-electron systems with spontaneously broken SU(2) symmetry, *Phys. Rev. B* **104**, 085120 (2021).
- [18] Ehsan Khatami, Three-dimensional Hubbard model in the thermodynamic limit, *Phys. Rev. B* **94**, 125114 (2016).
- [19] Lorenzo Del Re, Two-particle self-consistent approach for broken symmetry phases, [arXiv:2312.16280](https://arxiv.org/abs/2312.16280).
- [20] Leticia Tarruell and Laurent Sanchez-Palencia, Quantum simulation of the Hubbard model with ultracold fermions in optical lattices, *C.R. Phys.* **19**, 365 (2018).
- [21] Russell A. Hart, Pedro M. Duarte, Tsung-Lin Yang, Xinxing Liu, Thereza Paiva, Ehsan Khatami, Richard T. Scalettar, Nandini Trivedi, David A. Huse, and Randall G. Hulet, Observation of antiferromagnetic correlations in the Hubbard model with ultracold atoms, *Nature (London)* **519**, 211 (2015).
- [22] Anton Mazurenko, Christie S. Chiu, Geoffrey Ji, Maxwell F. Parsons, Márton Kanász-Nagy, Richard Schmidt, Fabian Grusdt, Eugene Demler, Daniel Greif, and Markus Greiner, A cold-atom Fermi-Hubbard antiferromagnet, *Nature (London)* **545**, 462 (2017).
- [23] Daniel Greif, Gregor Jotzu, Michael Messer, Rémi Desbuquois, and Tilman Esslinger, Formation and dynamics of antiferromagnetic correlations in tunable optical lattices, *Phys. Rev. Lett.* **115**, 260401 (2015).
- [24] Lawrence W Cheuk, Matthew A Nichols, Katherine R Lawrence, Melih Okan, Hao Zhang, Ehsan Khatami, Nandini Trivedi, Thereza Paiva, Marcos Rigol, and Martin W Zwierlein, Observation of spatial charge and spin correlations in the 2D Fermi-Hubbard model, *Science* **353**, 1260 (2016).
- [25] Peter T Brown, Debayan Mitra, Elmer Guardado-Sanchez, Peter Schauß, Stanimir S Kondov, Ehsan Khatami, Thereza Paiva, Nandini Trivedi, David A Huse, and Waseem S Bakr, Spin-imbalance in a 2D Fermi-Hubbard system, *Science* **357**, 1385 (2017).
- [26] Joannis Koepsell, Jayadev Vijayan, Pimonpan Sompert, Fabian Grusdt, Timon A Hilker, Eugene Demler, Guillaume Salomon, Immanuel Bloch, and Christian Gross, Imaging magnetic polarons in the doped Fermi-Hubbard model, *Nature (London)* **572**, 358 (2019).
- [27] Marcell Gall, Nicola Wurz, Jens Samland, Chun Fai Chan, and Michael Köhl, Competing magnetic orders in a bilayer Hubbard model with ultracold atoms, *Nature (London)* **589**, 40 (2021).
- [28] Pimonpan Sompert, Sarah Hirthe, Dominik Bourgund, Thomas Chalopin, Julian Bibo, Joannis Koepsell, Petar Bojović, Ruben Verresen, Frank Pollmann, Guillaume Salomon *et al.*, Realizing the symmetry-protected Haldane phase in Fermi-Hubbard ladders, *Nature (London)* **606**, 484 (2022).
- [29] Nikolai V. Prokof'ev and Boris V. Svistunov, Polaron problem by diagrammatic quantum Monte Carlo, *Phys. Rev. Lett.* **81**, 2514 (1998).
- [30] Kris Van Houcke, Evgeny Kozik, Nikolay Prokof'ev, and Boris Svistunov, Diagrammatic Monte Carlo, *Phys. Procedia* **6**, 95 (2010).
- [31] E. Kozik, K. Van Houcke, E. Gull, L. Pollet, N. Prokof'ev, B. Svistunov, and M. Troyer, Diagrammatic Monte Carlo for correlated fermions, *Europhys. Lett.* **90**, 10004 (2010).
- [32] Riccardo Rossi, Determinant diagrammatic Monte Carlo algorithm in the thermodynamic limit, *Phys. Rev. Lett.* **119**, 045701 (2017).
- [33] R. Rossi, N. Prokof'ev, B. Svistunov, K. Van Houcke, and F. Werner, Polynomial complexity despite the fermionic sign, *Europhys. Lett.* **118**, 10004 (2017).
- [34] Fedor Šimkovic, J. P. F. LeBlanc, Aaram J. Kim, Youjin Deng, N. V. Prokof'ev, B. V. Svistunov, and Evgeny Kozik, Extended crossover from a Fermi liquid to a quasiantiferromagnet in the half-filled 2D Hubbard model, *Phys. Rev. Lett.* **124**, 017003 (2020).
- [35] Thomas Schäfer, Nils Wentzell, Fedor Šimkovic, Yuan-Yao He, Cornelia Hille, Marcel Klett, Christian J. Eckhardt, Behnam Arzhang, Viktor Harkov, François-Marie Le Régent, Alfred Kirsch, Yan Wang, Aaram J. Kim, Evgeny Kozik, Evgeny A. Stepanov, Anna Kauch, Sabine Andergassen, Philipp Hansmann, Daniel Rohe, Yuri M. Vilk, James P. F. LeBlanc, Shiwei Zhang, A.-M. S. Tremblay, Michel Ferrero, Olivier Parcollet, and Antoine Georges, Tracking the footprints of spin fluctuations: A multiMethod, multiMessenger study of the two-dimensional Hubbard model, *Phys. Rev. X* **11**, 011058 (2021).
- [36] Aaram J. Kim, Fedor Simkovic, and Evgeny Kozik, Spin and charge correlations across the metal-to-insulator crossover in the half-filled 2D Hubbard model, *Phys. Rev. Lett.* **124**, 117602 (2020).
- [37] Connor Lenihan, Aaram J. Kim, Fedor Šimkovic IV, and Evgeny Kozik, Entropy in the non-Fermi-liquid regime of

- the doped 2D Hubbard model, *Phys. Rev. Lett.* **126**, 105701 (2021).
- [38] J. P. F. LeBlanc, Andrey E. Antipov, Federico Becca, Ireneusz W. Bulik, Garnet Kin-Lic Chan, Chia-Min Chung, Youjin Deng, Michel Ferrero, Thomas M. Henderson, Carlos A. Jiménez-Hoyos, E. Kozik, Xuan-Wen Liu, Andrew J. Millis, N. V. Prokof'ev, Mingpu Qin, Gustavo E. Scuseria, Hao Shi, B. V. Svistunov, Luca F. Tocchio, I. S. Tupitsyn, Steven R. White, Shiwei Zhang, Bo-Xiao Zheng, Zhenyue Zhu, and Emanuel Gull, Solutions of the two-dimensional Hubbard model: Benchmarks and results from a wide range of numerical Algorithms, *Phys. Rev. X* **5**, 041041 (2015).
- [39] Wei Wu, Michel Ferrero, Antoine Georges, and Evgeny Kozik, Controlling Feynman diagrammatic expansions: Physical nature of the pseudogap in the two-dimensional Hubbard model, *Phys. Rev. B* **96**, 041105(R) (2017).
- [40] Riccardo Rossi, Fedor Šimkovic, and Michel Ferrero, Renormalized perturbation theory at large expansion orders, *Europhys. Lett.* **132**, 11001 (2020).
- [41] Fedor Šimkovic, Riccardo Rossi, and Michel Ferrero, The weak, the Strong and the long correlation regimes of the two-dimensional Hubbard model at finite temperature, *Phys. Rev. Res.* **4**, 043201 (2022).
- [42] Connor Lenihan, Aaram J. Kim, IV. Šimkovic, Fedor, and Evgeny Kozik, Evaluating second-order phase transitions with diagrammatic Monte Carlo: Néel transition in the doped three-dimensional Hubbard model, *Phys. Rev. Lett.* **129**, 107202 (2022).
- [43] Fedor Simkovic, Riccardo Rossi, Antoine Georges, and Michel Ferrero, Origin and fate of the pseudogap in the doped Hubbard model, [arXiv:2209.09237](https://arxiv.org/abs/2209.09237).
- [44] Rosario E. V. Profumo, Christoph Groth, Laura Messio, Olivier Parcollet, and Xavier Waintal, Quantum Monte Carlo for correlated out-of-equilibrium nanoelectronic devices, *Phys. Rev. B* **91**, 245154 (2015).
- [45] Fedor Šimkovic, Riccardo Rossi, and Michel Ferrero, Efficient one-loop-renormalized vertex expansions with connected determinant diagrammatic Monte Carlo, *Phys. Rev. B* **102**, 195122 (2020).
- [46] Aaram J. Kim, Nikolay V. Prokof'ev, Boris V. Svistunov, and Evgeny Kozik, Homotopic action: A pathway to convergent diagrammatic theories, *Phys. Rev. Lett.* **126**, 257001 (2021).
- [47] James P. F. LeBlanc, Kun Chen, Kristjan Haule, Nikolay V. Prokof'ev, and Igor S. Tupitsyn, Dynamic response of the electron gas: Towards the exact exchange-correlation kernel, *Phys. Rev. Lett.* **129**, 246401 (2022).
- [48] R. Rossi, T. Ohgoe, K. Van Houcke, and F. Werner, Resummation of diagrammatic series with zero convergence radius for strongly correlated fermions, *Phys. Rev. Lett.* **121**, 130405 (2018).
- [49] K. Chen and K. Haule, A combined variational and diagrammatic quantum Monte Carlo approach to the many-electron problem, *Nat. Commun.* **10**, 3725 (2019).
- [50] R. Rossi, F. Werner, N. Prokof'ev, and B. Svistunov, Shifted-action expansion and applicability of dressed diagrammatic schemes, *Phys. Rev. B* **93**, 161102(R) (2016).
- [51] Igor S. Tupitsyn and Nikolay V. Prokof'ev, Phase diagram topology of the Haldane-Hubbard-Coulomb model, *Phys. Rev. B* **99**, 121113(R) (2019).
- [52] Yuan Huang, Kun Chen, Youjin Deng, Nikolay Prokof'ev, and Boris Svistunov, Spin-ice state of the quantum Heisenberg antiferromagnet on the pyrochlore lattice, *Phys. Rev. Lett.* **116**, 177203 (2016).
- [53] G. Spada, R. Rossi, F. Simkovic, R. Garioud, M. Ferrero, K. Van Houcke, and F. Werner, High-order expansion around BCS theory, [arXiv:2103.12038](https://arxiv.org/abs/2103.12038).
- [54] Fedor Šimkovic and Riccardo Rossi, Many-configuration Markov-chain Monte Carlo, [arXiv:2102.05613](https://arxiv.org/abs/2102.05613).
- [55] Kent Griffin and Michael J. Tsatsomeros, Principal minors, Part I: A method for computing all the principal minors of a matrix, *Linear Algebra Appl.* **419**, 107 (2006).
- [56] Fedor Šimkovic and Michel Ferrero, Fast principal minor algorithms for diagrammatic Monte Carlo, *Phys. Rev. B* **105**, 125104 (2022).
- [57] George A. Baker, Application of the Padé approximant method to the investigation of some magnetic properties of the Ising model, *Phys. Rev.* **124**, 768 (1961).
- [58] Fedor Šimkovic and Evgeny Kozik, Determinant Monte Carlo for irreducible Feynman diagrams in the strongly correlated regime, *Phys. Rev. B* **100**, 121102(R) (2019).
- [59] See Supplemental Material at <http://link.aps.org/supplemental/10.1103/PhysRevLett.132.246505> which includes Refs. [60–62].
- [60] Jean-Loïc Kneur, Marcus B. Pinto, and Rudnei O. Ramos, Asymptotically improved convergence of optimized perturbation theory in the Bose-Einstein condensation problem, *Phys. Rev. A* **68**, 043615 (2003).
- [61] P. M. Stevenson, Optimized perturbation theory, *Phys. Rev. D* **23**, 2916 (1981).
- [62] R. L. S. Farias, G. Krein, and Rudnei O. Ramos, Applicability of the linear δ expansion for the $\lambda\phi^4$ field theory at finite temperature in the symmetric and broken phases, *Phys. Rev. D* **78**, 065046 (2008).
- [63] Julian Stobbe and Georg Rohringer, Consistency of potential energy in the dynamical vertex approximation, *Phys. Rev. B* **106**, 205101 (2022).
- [64] J. C. Slater, Magnetic effects and the Hartree-Fock equation, *Phys. Rev.* **82**, 538 (1951).
- [65] Anders W. Sandvik, Critical temperature and the transition from quantum to classical order parameter fluctuations in the three-dimensional Heisenberg antiferromagnet, *Phys. Rev. Lett.* **80**, 5196 (1998).
- [66] Massimo Campostrini, Martin Hasenbusch, Andrea Pelissetto, Paolo Rossi, and Ettore Vicari, Critical exponents and equation of state of the three-dimensional Heisenberg universality class, *Phys. Rev. B* **65**, 144520 (2002).
- [67] T. Schäfer, A. A. Katanin, K. Held, and A. Toschi, Interplay of correlations and Kohn anomalies in three dimensions: Quantum criticality with a twist, *Phys. Rev. Lett.* **119**, 046402 (2017).
- [68] Antoine Georges and Werner Krauth, Physical properties of the half-filled Hubbard model in infinite dimensions, *Phys. Rev. B* **48**, 7167 (1993).

- [69] F. Werner, O. Parcollet, A. Georges, and S.R. Hassan, Interaction-induced adiabatic cooling and antiferromagnetism of cold fermions in optical lattices, *Phys. Rev. Lett.* **95**, 056401 (2005).
- [70] Lorenzo De Leo, Corinna Kollath, Antoine Georges, Michel Ferrero, and Olivier Parcollet, Trapping and cooling fermionic atoms into Mott and Néel states, *Phys. Rev. Lett.* **101**, 210403 (2008).
- [71] E. V. Gorelik, I. Titvinidze, W. Hofstetter, M. Snoek, and N. Blümer, Néel transition of lattice fermions in a harmonic trap: A real-space dynamic mean-field study, *Phys. Rev. Lett.* **105**, 065301 (2010).
- [72] Sebastian Fuchs, Emanuel Gull, Lode Pollet, Evgeni Burovski, Evgeny Kozik, Thomas Pruschke, and Matthias Troyer, Thermodynamics of the 3D Hubbard model on approaching the Néel transition, *Phys. Rev. Lett.* **106**, 030401 (2011).
- [73] E. Gull, P. Werner, X. Wang, M. Troyer, and A. J. Millis, Local order and the gapped phase of the Hubbard model: A plaquette dynamical mean-field investigation, *Europhys. Lett.* **84**, 37009 (2008).
- [74] C. Taranto, G. Sangiovanni, K. Held, M. Capone, A. Georges, and A. Toschi, Signature of antiferromagnetic long-range order in the optical spectrum of strongly correlated electron systems, *Phys. Rev. B* **85**, 085124 (2012).
- [75] L. Fratino, P. Sémon, M. Charlebois, G. Sordi, and A.-M. S. Tremblay, Signatures of the Mott transition in the antiferromagnetic state of the two-dimensional Hubbard model, *Phys. Rev. B* **95**, 235109 (2017).
- [76] E. V. Gorelik, I. Titvinidze, W. Hofstetter, M. Snoek, and N. Blümer, Néel transition of lattice fermions in a harmonic trap: A real-space dynamic mean-field study, *Phys. Rev. Lett.* **105**, 065301 (2010).
- [77] Anne-Marie Daré, Y.M. Vilks, and A.M.S. Tremblay, Crossover from two- to three-dimensional critical behavior for nearly antiferromagnetic itinerant electrons, *Phys. Rev. B* **53**, 14236 (1996).